How Solvent Controls Electronic Energy Transfer and Light Harvesting: Toward a Quantum-Mechanical Description of Reaction Field and Screening Effects

Carles Curutchet,*,† Gregory D. Scholes,‡ Benedetta Mennucci,§ and Roberto Cammi†

Dipartimento di Chimica Generale ed Inorganica, Chimica Analitica e Chimica Fisica, Università di Parma, Parco Area delle Scienze, I-43100 Parma, Italy, Department of Chemistry, 80 Saint George Street, Institute for Optical Sciences and Centre for Quantum Information and Quantum Control, University of Toronto, Toronto, Ontario M5S 3H6 Canada, and Dipartimento di Chimica e Chimica Industriale, Università di Pisa, via Risorgimento 35, 56126 Pisa, Italy

Received: July 11, 2007; In Final Form: September 6, 2007

This paper presents a quantum-mechanical study of electronic energy transfer (EET) coupling on over 100 pairs of chromophores taken from photosynthetic light-harvesting antenna proteins. Solvation effects due to the protein, intrinsic waters, and surrounding medium are analyzed in terms of screening and reaction field contributions using a model developed recently that combines a linear response approach with the polarizable continuum model (PCM). We find that the screening of EET interactions is quite insensitive to the quantum-mechanical treatment adopted. In contrast, it is greatly dependent on the geometrical details (distance, shape, and orientation) of the chromophore pair considered. We demonstrate that implicit (reaction field) as well as screening effects are dictated mainly by the optical dielectric properties of the host medium, while the effect of the static properties is substantially less important. The empirical distance-dependent screening function we proposed in a recent letter (Scholes, G. D.; Curutchet, C.; Mennucci, B.; Cammi, R.; Tomasi, J. *J. Phys. Chem. B* **2007**, *111*, 6978−6982) is analyzed and compared to other commonly used screening factors. In addition, we show that implicit medium effects on the coupling, resulting from changes in the transition densities upon solvation, are strongly dependent on the particular system considered, thus preventing the possibility of defining a general empirical expression for such an effect.

1. Introduction

After absorption of light, the excitation energy of a chromophore can be efficiently transferred to another chromophore up to distances of several tens of angstroms by the process of electronic energy transfer (EET).[1] EET has been studied extensively and is intrinsic to a wide range of applications, for example, the amplification of fluorescence-based sensors,[2] the optimization of organic light-emitting diodes,[3] or the measurement of distances in biological systems—even in vivo—because the rate of EET depends sensitively on the donor−acceptor separation.[4−6] This photophysical process is ubiquitous in nature, playing a key role in the light-harvesting machinery of photosynthesis, where hundreds of special antennae molecules are used to collect light and transfer the absorbed energy toward reaction centers where charge separation occurs.[7−13] Inspired by these systems, researchers have designed and employed artificial antennae for the capture and energy conversion of light.[14−18]

Applications that utilize EET have been optimized based on theories to predict the dynamics of EET. Alternatively, fundamental studies of structurally well-defined systems are used to learn more about EET mechanisms and dynamics. The principal theory relating experimental observables to the mechanisms of EET was formulated by Förster more than 50 years ago[19] and is still widely used today. In general, predicting the dynamics of EET requires four ingredients: spectral factors for the donor and acceptor molecules,[19] electronic coupling between them,[20] identification of possible coherence effects,[21−24] and account of the environment as a dielectric medium.[25−30] In particular, the Förster (weak coupling) formula for predicting the EET rate from a donor molecule D to an acceptor molecule A is given by

$$k = \frac{2\pi}{\hbar} |V|^2 J \tag{1}$$

where J is the spectral overlap factor[1] and V is the electronic coupling between D and A transition densities.

In most photosyntetic systems, however, pigments are so closely packed that one has to go beyond Förster theory and consider a delocalization of excited states. In this case, the degree of delocalization dictating the dynamics of EET or the optical spectra are also strongly dependent on the electronic coupling V between chromophores.

In this context, as in the Förster model, V is often defined as sV_s, where V_s indicates the direct interaction between the D and A and s is the solvent screening factor and equals $1/n^2$, n being the refractive index of the medium. The characteristic R^{-6} distance decay of the EET rate in Förster theory arises from the dipole−dipole approximation adopted for the V_s term. Alternatively, it is also common to consider effective dipole strengths, which only implicitly take account of the screening of the interactions.

There are, however, several aspects that can limit the applicability of the popular Förster expression for the coupling.

* Corresponding author. E-mail: carles@dcci.unipi.it.
† Università di Parma.
‡ University of Toronto.
§ Università di Pisa.

10.1021/jp075411h CCC: $37.00
Published on Web 11/01/2007

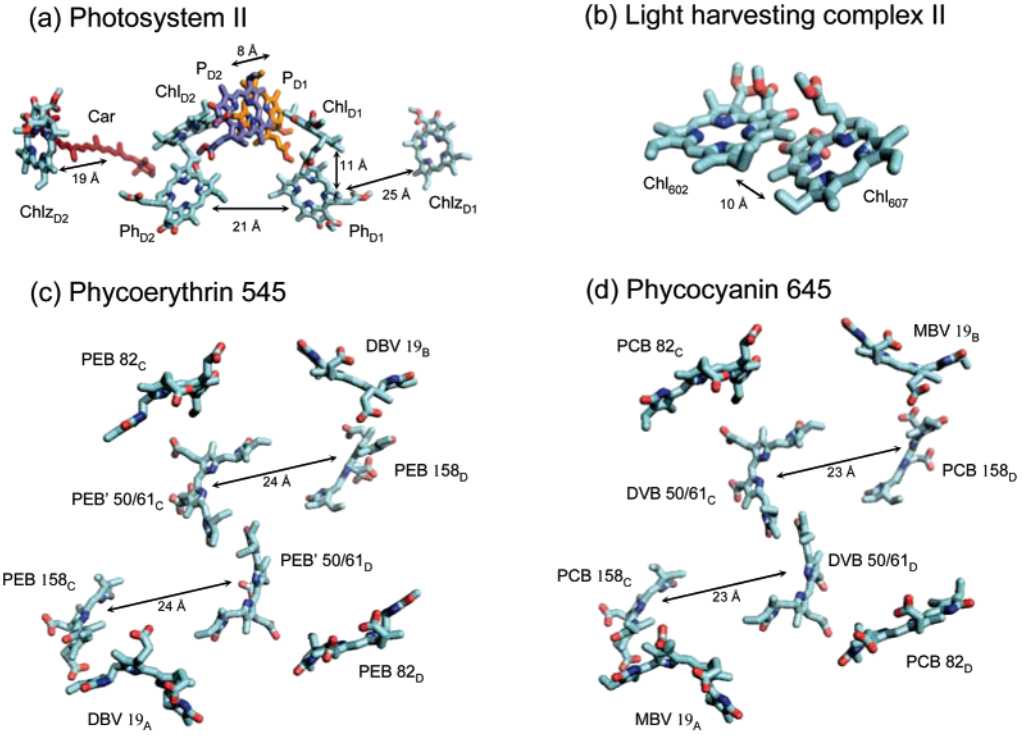

Figure 1. Light-absorbing molecules studied in this work. The structural models correspond to (a) photosystem II (PSII) from the cyanobacteria *T. elongatus*, (b) the peripheral light-harvesting complex (LHCII) from pea, and the (c) phycoerythrin 545 (PE545) and (d) phycocyanin 645 (PC645) light-harvesting antennae from the cryptophyte algae *Rhodomonas CS24* and *Choomonas CCMP270*.

The most obvious is the possible breakdown of the dipole−dipole approximation when the separation between the chromophores is small. Modern theories based on ab initio or semiempirical methods, for example, overcome the dipole−dipole approximation by using more accurate quantum-mechanical descriptions of the interacting chromophores.[1,31−36] Concomitant with improvements in the treatment of electronic coupling, it is necessary to elucidate the screening of those interactions by the surroundings. That aspect of EET theories has received little attention, despite its importance. The simple screening model, $s = 1/n^2$, originally proposed by Förster is used.[19] This model predicts a reduction of the EET rate (by a factor of ∼4) regardless of how the donor and acceptor are oriented and positioned. In a similar way, the use of effective dipole strengths assumes that the screening is constant in the estimation of couplings for different pairs of chromophores. This is clearly a significant approximation, and it has already been suggested that at short D/A separations, when the surrounding medium is excluded from the intermolecular region, the environment should play a more complex role on the coupling. That may lead to a significant reduction of the screening or even to an enhancement of the interaction.[25] It could be expected, for example, that the screening might be distance-dependent, in analogy with empirical distance-dependent screening functions used to model electrostatic interactions in proteins and nucleic acids.[37] The importance of this issue has already been raised in the literature,[25,38−40] but until now the complexity of the problem has prevented a detailed quantum-mechanical exploration in realistic systems. In this context, however, it is worth noting a recent study by Adolphs and Renger[41] on the role of the protein matrix in the interactions between the chromophores of the Fenna−Matthews−Olson (FMO) complex. In that study, electronic couplings were obtained from atomic transition monopole (TM) charges and the effect of the environment was introduced by numerically solving the Poisson equation by a finite difference method.

The treatment of screening of EET in light-harvesting proteins is clearly a complex problem. In contrast to standard solvents, protein environments are heterogeneous and largely anisotropic. Measurements of time-dependent fluorescence Stokes shifts[42] and molecular dynamics (MD) simulations[43] have indeed demonstrated that polar solvation dynamics in such systems, arising from both interactions with protein residues and with the solvent, are position-dependent and highly heterogeneous. Depending on the particular protein or protein site, for example, static dielectric permittivities ϵ ranging from 4 to 40 have been estimated from MD simulations.[44−47] Because of the dynamic nature of the interaction promoting EET, however, the screening is affected mainly by the optical dielectric permittivity ϵ_{opt}, that is, the square of the refractive index n, much less variable than ϵ as n ranges from 1.3 to 1.6 in typical relevant environments. Thus, the essence of the problem regarding the screening of EET should be captured by using a reasonable value of ϵ_{opt} along with a modern continuum solvation model overcoming the strong approximations of the Förster screening factor. Recently, we have developed a quantum-mechanical model that combines a linear response (LR) approach with a polarizable solvation continuum model to describe EET couplings.[27,48] This methodology captures key features of the problem, such as an accurate calculation of excited states, the shape of molecules, and the response of the surrounding medium to charge and, importantly, transition densities.

In a recent letter,[49] we have applied our model of EET to examine the screening for a set of over 100 pairs of chromophores (chlorophylls, carotenoids and bilins) taken from structural models of photosynthetic proteins (see Figure 1). In that study, we have found a striking exponential attenuation of the screening factor s at separations less than about 20 Å, thus interpolating between the limits of no apparent screening and a significant attenuation of the EET rate. This observation reveals a previously unidentified contribution to the distance dependence of the EET rate, which has particularly important consequences

for the development of quantitative EET models as those actively pursued in the study of photosynthetic light-harvesting systems and conjugated polymers.[3,7,8,41,50]

In the present work, we extend and complete that study by analyzing the main aspects affecting the EET coupling between protein solvated chromophores: not only the distance dependence of the screening but also the sensitivity on the shape and orientation of the interacting chromophores, on the dielectric properties of the environment, and on the quantum-mechanical level of theory, including eventual mutual polarization effects between the chromophores. In addition, we quantify the consequences derived from the use of the approximations most commonly adopted in theoretical models of EET such as the point-dipole approximation (PDA), the use of Förster's simple screening factor, and the neglect of implicit solvation effects.

The paper is organized as follows. In Section 2, we briefly describe the theory underlying the model. Then, in Section 3.2 we discuss the sensitivity of our results on the level of theory and on eventual mutual polarization effects between the monomers. In Section 3.3, we illustrate the dependence of the solvent screening on the shape, orientation, and separation between the interacting molecules, and in Section 3.4 we explore the effects of changing the dielectric properties of the environment. Finally, in Section 3.5 we pass on discussing the role of the surrounding medium on biological EET phenomena by analyzing the results obtained for photosynthetic proteins.

2. Methods

By definition, the electronic coupling in EET is a long-range dynamic interaction between two transition densities. This quantum-mechanical nature of the coupling makes it difficult to obtain an accurate estimation of its value for real systems including the effect of the environment. In the present work, we adopt a quantum-mechanical description of the problem and we describe the environment effects through the *integral equation formalism* (IEF)[51] version of the polarizable continuum model (PCM).[52] In quantum-mechanical continuum solvation models,[53,54] the molecular system under scrutiny (the "solute") is described at a quantum-mechanical level, while the solvent is approximated as a structureless polarizable continuum characterized by its macroscopic dielectric properties. The resulting electrostatic problem determined by the Laplace−Poisson equation (with appropriate boundary conditions) can be solved in different ways. In the IEFPCM model, this is obtained by describing the permittivity-dependent polarization induced by the solute on the environment, the *reaction field*, as a set of *apparent surface charges* (ASC) distributed on the surface of the molecular-shaped cavity containing the solute. Such a cavity is built from a superposition of interlocked atom-centered spheres located at selected nuclei, which are obtained from properly scaled van der Waals radii. To obtain a mutually polarized solute−environment system, the two coupled equations to be solved are

$$\{\hat{H}^0 + \sum_k q(s_k;\epsilon)\hat{V}^{\mathrm{el}}(\mathbf{s}_k)\}|\Psi\rangle = E|\Psi\rangle \qquad (2)$$

$$q(s_k;\epsilon) = -\sum_l \mathbf{K}_{kl}[\epsilon]\{\langle\Psi|\hat{V}^{\mathrm{el}}(\mathbf{s}_l)|\Psi\rangle + V^{\mathrm{N}}(\mathbf{s}_l)\} \qquad (3)$$

where q are the ASCs located at the center s_k of the discrete surface elements (*tesserae*) in which the cavity surface is partitioned. In the equations above, r is the electronic coordinate, the k, l indices run on the total number of tesserae, $\mathbf{K}[\epsilon]$ is the IEFPCM matrix,[54] $\langle\Psi|\hat{V}^{\mathrm{el}}(\mathbf{s}_l)|\Psi\rangle$ and $V^{\mathrm{N}}(\mathbf{s}_l)$ indicate the electrostatic potential due to the solute electrons and nuclei on the tesserae, respectively, and ϵ is the static dielectric constant of the solvent.

The advantage of such a strategy with respect to methods representing the solvent molecules explicitly regards its reduced computational cost as well as the ability to directly obtain an ensemble average of the solute−environment interactions. In addition, this approach allows the treatment of dynamic processes such as electronic transitions in the solute by taking into account the dynamic response of the medium. In polar solvents, in fact, fast changes in the solute charge distribution can give rise to a delay in its response or equivalently to a nonequilibrium polarization. Within the IEFPCM, this is obtained by assuming that the corresponding changes in the apparent charges (and the resulting dynamic part of the reaction field) are determined by the optical permittivity (ϵ_{opt}) instead of the static one (ϵ).

Our model for the environment effects on the EET coupling, described in detail in ref 27, is an application of this nonequilibrium scheme within a quantum-mechanical linear response (LR) approach.[55] In this framework, the ground-state properties of the "solute" are determined by the static permittivity of the medium, whereas the dynamical changes on the environment polarization arising from electronic transitions are determined by the optical one. As a result, transition energies and densities are directly affected by ϵ_{opt} and only indirectly by ϵ (see ref 55 for more details).

In addition, an approximate solution of the LR scheme is introduced in which the D/A interaction is considered as a perturbation and the electronic coupling is obtained from the transition densities of the single chromophores in the absence of their interaction. To first-order, the electronic coupling, V, is obtained as a sum of two terms, the direct (or Coulombic-exchange) coupling, implicitly modified by the medium (V_{s}), and the contribution involving the explicit solvent effect (V_{explicit})

$$V = V_{\mathrm{s}} + V_{\mathrm{explicit}} \qquad (4)$$

$$V_{\mathrm{s}} = \int \mathrm{d}\mathbf{r} \int \mathrm{d}\mathbf{r}'\, \rho_{\mathrm{A}}^{\mathrm{T}*}(\mathbf{r}')\left(\frac{1}{|\mathbf{r}'-\mathbf{r}|} + g_{xc}(\mathbf{r}',\mathbf{r})\right)\rho_{\mathrm{D}}^{\mathrm{T}}(\mathbf{r}) + - \omega_{\mathrm{D/A}} \int \mathrm{d}\mathbf{r}\, \rho_{\mathrm{A}}^{\mathrm{T}*}(\mathbf{r})\,\rho_{\mathrm{D}}^{\mathrm{T}}(\mathbf{r}) \qquad (5)$$

$$V_{\mathrm{explicit}} = \sum_k \left(\int \mathrm{d}\mathbf{r}\, \rho_{\mathrm{A}}^{\mathrm{T}*}(\mathbf{r})\frac{1}{|\mathbf{r}-\mathbf{s}_k|}\right) q(s_k;\epsilon_\omega,\rho_{\mathrm{D}}^{\mathrm{T}}) \qquad (6)$$

where $\rho_{\mathrm{D}}^{\mathrm{T}}$ and $\rho_{\mathrm{A}}^{\mathrm{T}}$ indicate transition densities of the solvated systems D and A, respectively, in the absence of their interaction, $g_{xc}(\mathbf{r}',\mathbf{r})$ is the exchange eventually plus correlation (if a DFT description is used) kernel, and ϵ_ω is the frequency-dependent dielectric permittivity of the medium. In the EET process, ϵ_ω will coincide with the optical permittivity ϵ_{opt}, that is, the square of the refractive index n.

It is worth noting that at close D/A separations, when the chromophores are enclosed in a common cavity (see Figure 3 in ref 49), the three steps needed to obtain the coupling (the calculation of the D and A transition properties and of their interaction) are performed in the same dimer cavity. This avoids artificial enhancements of the medium-induced polarization of $\rho_{\mathrm{D}}^{\mathrm{T}}$ and $\rho_{\mathrm{A}}^{\mathrm{T}}$.

In eq 5, V_{s} describes a chromophore−chromophore Coulomb and exchange-correlation interaction (through the kernel g_{xc}) corrected by an overlap contribution. This term, shown schematically in Figure 2, is the only present for isolated systems. Here, however, the values of the transition densities $\rho_{\mathrm{D}}^{\mathrm{T}}$ and $\rho_{\mathrm{A}}^{\mathrm{T}}$

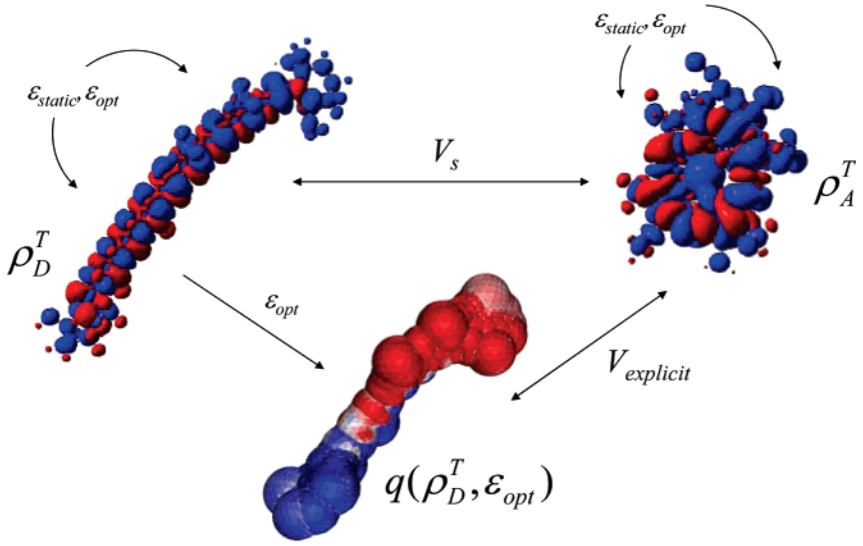

Figure 2. Graphical representation of the direct interaction between the transition densities ρ_D^T and ρ_A^T (V_s) and that mediated by the reaction potential generated in response to ρ_D^T ($V_{explicit}$). The marked dipolar distribution of the reaction potential (red and blue zones) highlights the strong dipolar character of the transition.

can be significantly modified by the reaction field produced by the polarized medium, hence also altering their direct interaction. This effect of the medium is denoted here as the *implicit* solvent effect and can be accounted for in the Förster theory by using the spectral information measured in the medium of interest. In addition, the solvent explicitly enters into the definition of the coupling through the term $V_{explicit}$ in eq 6, which describes an indirect interaction between the two chromophores mediated by the medium. This term, denoted as the *explicit* solvent effect, generally leads to an overall reduction (i.e., *screening*) of the D/A coupling and is obtained as the interaction between ρ_A^T and the solvent reaction potential generated in response to ρ_D^T (see Figure 2). Within this framework, we can define the solvent screening factor as in eq 7:

$$s = V/V_s = (V_s + V_{explicit})/V_s \tag{7}$$

This factor s can thus be directly compared to the $s = 1/n^2$ value used in Förster's model, which assumes an interaction between (infinitely thin) point dipoles, or to the prediction of Onsager theory, $s = 3/(2n^2 + 1)$, which considers the dipoles as contained in spherical cavities. In order to illustrate the connection between the PCM formalism and the earlier literature about solvent effect on EET coupling, in the Appendix we report a detailed derivation of the Onsager model and we discuss its correspondence with the implicit/explicit PCM contributions.

The perturbative LR-IEFPCM model has been applied to study EET between molecules in liquid solutions[27,48,56] and at liquid/gas interfaces,[57] and to the excitonic splitting in conjugated molecular materials.[58] In these papers, the validity of the approximations introduced in this approach have been confirmed by comparison with "supermolecule" calculations, that is, where the electronic coupling is obtained from the energy splitting induced by the D/A interaction in the dimer excited states.

With respect to these supermolecule calculations, the perturbative model presents significant advantages. An obvious one is that it is much more computationally efficient because it only requires excited-state calculations for each single chromophore. In addition, it avoids the contribution of other excited states to the dimeric splitting in nonsymmetric pairs, or common problems associated with TDDFT methods in the description of electronic excitations in D/A systems.[48,59] Finally, the perturbative model allows us to dissect the various contributions to the electronic coupling, in particular, the effect of the surrounding medium either on the properties of the chromophores and on their interaction.

3. Results and Discussion

We have calculated electronic couplings both in vacuum and in the dielectric environment between over 100 pairs of chromophores found in four different photosynthetic proteins, Figure 1, which include photosystem II (PSII) from the cyanobacteria *T. elongatus*,[60] the phycoerythrin 545 (PE545) and phycocyanin 645 (PC645) light-harvesting antennae from the cryptophyte algae[61] *Rhodomonas CS24* and *Choomonas CCMP270*, and the peripheral light-harvesting complex (LHCII) from pea.[62]

We consider EET between the brightest states of the molecules, namely the Q_y state of chlorophylls and pheophytins, the S_2 state of carotenoids (β-carotene) and the S_1 state of bilins, all of them characterized by a dominant HOMO $\rightarrow$ LUMO contribution while chlorophylls and pheophytins Q_y state is characterized by a HOMO $\rightarrow$ LUMO and a HOMO $-$ 1 $\rightarrow$ LUMO + 1 contributions. The V_s couplings reported arise mainly from Coulomb interactions, and only for two pairs exchange contributions represent slightly more than 1% of V_s ($\sim$2$-$3%).

Before reporting the analysis on the total data set, we explore the sensitivity of the electronic coupling and the corresponding screening on key aspects of the model, namely the quantum-mechanical level of description, the shape of the chromophores, their relative orientation and interchromophoric (center-to-center) distance, and the dielectric properties of the environment. To this end, we have selected three pairs from the data set, the $P_{D1}-P_{D2}$, $Chl_{D1}-Ph_{D1}$, and $Car-Chlz_{D2}$ dimers of PSII.

3.1. Computational Details. Geometries were obtained from reported structural models. Hydrogens were added and optimized at the HF/6-31G level keeping all of the other atoms frozen. For the $P_{D1}-P_{D2}$, $Chl_{D1}-Ph_{D1}$, and $Car-Chlz_{D2}$ dimers, additional distance-dependent coupling profiles were obtained by enlarging the interchromophore (center-to-center) separation. All quantum chemical calculations of the coupling were performed at the CI-singles/6-31G level using a local version of the

TABLE 1: CIS/6-31G Direct, Explicit, and Total Coupling (in cm^{-1}), and Screening Factor *s* for $P_{D1}-P_{D2}$, $Chl_{D1}-Ph_{D1}$, and $Car-Chlz_{D2}$ Dimers of PSII

	CIS				CIS + ESP			
	V_s	$V_{explicit}$	V	s	V_s	$V_{explicit}$	V	s
$P_{D1}-P_{D2}$ ($R = 8.0$)	181	−38	143	0.79	178	−37	141	0.79
$Chl_{D1}-Ph_{D1}$ ($R = 10.7$)	127	−33	94	0.74	126	−33	93	0.74
$Car-Chlz_{D2}$ ($R = 18.9$)	118	−56	61	0.52	118	−56	61	0.52

Gaussian 03 code[63] properly modified to perform the calculation of the electronic couplings.

The calculations in the dielectric medium were performed using the IEFPCM solvation model. Molecular cavities were obtained in terms of interlocking spheres centered on selected nuclei. The chosen radii were 2.525 Å for methyl groups, 2.325 Å for methylene groups, 2.125 Å for CH groups, 1.925 Å for carbon atoms, 1.830 Å for nitrogen atoms, 1.750 Å for oxygen atoms, 1.511 Å for magnesium atoms, and 1.200 Å for hydrogen atoms bonded to N or O. These radii were obtained by applying the United Atom Topological Model to the atomic radii of the UFF force field[64] as implemented in the Gaussian 03 code.

To describe the dielectric properties of the environment (protein, intrinsic waters, and surrounding medium) around each chromophore, we have selected the values of 2 for optical permittivity (ϵ_{opt}) and 15 for the static one (ϵ). These values have been reported based on dielectric dispersion measurements of hydrated lysozime powders.[65] It is thought that these values describe the solvation dynamics of protein environments well. Indeed $\epsilon_{opt} \sim 2$ is a commonly adopted value for different kinds of proteins,[39−41,66−68] whereas ϵ is known to depend much more on the specific protein.[42−47] The precise determination of dielectric permittivities for complex chemical systems as proteins is a challenge at present, and it is not clear to what extent a single ϵ/ϵ_{opt} pair of parameters can capture complex solvation dynamics in such systems. This values can be considered a first approximation in this context, and in fact our focus here is not on the precise values of the couplings but rather on the behavior and trends obtained for the solvent screening factor. Indeed, we have checked the dependence of the solvent screening on the dielectric properties of the medium by examining various values of ϵ_{opt} and ϵ (Section 3.4).

3.2. Effects of the Quantum-Mechanical Level of Description. The LR-IEFPCM approach described in Section 2 is based on the assumption that a reliable and accurate evaluation of the coupling can be obtained using the transition densities of the two chromophores when not interacting (ρ_D^T and ρ_A^T in eqs 5 and 6). This assumption is an approximation as each monomer will affect the properties of the other and thus indirectly also their interaction with the environment and the coupling. The most straightforward way to check the significance of the polarization of a transition density by the presence of a nearby molecule is to introduce the effect of the second monomer in the calculation of each ρ_X^T using a set of standard point charges obtained by fitting the electrostatic potential representing the other monomer charge distribution (ESP charges).

In Table 1, we report the direct coupling (V_s), the contribution involving the explicit solvent effect ($V_{explicit}$), the total coupling, and the screening factor *s* for the three selected pairs when the properties of each chromophore are obtained in the absence or in presence of the HF/6-31G(d) ESP charges representing the second chromophore.

As can be seen, the effects caused by account of the other chromophore ESP charges are very small for all the three dimers. Some changes are visible on the direct and explicit contributions (and thus on the total coupling) while the screening factor *s* seems insensitive to the presence of the charges.

TABLE 2: Comparison of CIS/6-31G, CIS/6-31++G(d,p), and TDDFT(B3LYP)/6-31G Level of Calculations for the Screening Factor *s* of the $P_{D1}-P_{D2}$ Dimer with Respect to Their Center-to-Center Distance

R (Å)	CIS/6-31G	CIS/6-31++G(d,p)	B3LYP/6-31G
8	0.80	0.83	0.83
9	0.75	0.77	0.78
10	0.69	0.70	0.72
11	0.63	0.63	0.66
12	0.59	0.59	0.61
13	0.56	0.55	0.58
14	0.55	0.54	0.56
15	0.55	0.54	0.56
16	0.57	0.56	0.56

This low sensitivity of the screening with respect to the description used to obtain the transition properties of each chromophore is confirmed by further analysis in which we have modified the quantum-mechanical level of theory either by enlarging the basis set with the inclusion of both polarization and diffuse functions [6-31++G(d,p)] or by adopting a TDDFT description using the common B3LYP functional.[69]

In this case, we have analyzed the changes in the screening factor of the $P_{D1}-P_{D2}$ dimer with respect to their center-to-center distance starting from the value found in the PSII ($R =$ 8.0 Å). The results are reported in Table 2 for the CIS/6-31G, CIS/6-31++G(d,p), and TDDFT(B3LYP)/6-31G levels of calculation.

As can be seen from the results reported in Table 2, the screening factors obtained with a larger basis set and also a correlated quantum-mechanical description are very similar to the CIS/6-31G model. It is only at the shortest distances where screening factors are mildly method-dependent. It is concluded that *s* is very weakly dependent on the quality of the quantum-mechanical description of the transition densities, whereas it changes significantly with the separation of the interacting chromophores. As a matter of fact, distance is not the only geometrical parameter that strongly affects the screening. We find that orientation and shape are also relevant, as shown in the following section.

3.3. Shape, Orientation, and Distance Dependence. In Figure 3, we show the solvent screening profiles obtained by varying the center-to-center distance for the three dimers. The initial geometries, with separations of 8.0, 10.7, and 18.9 Å, respectively, are taken from published structural models and are represented in the figure along with the associated IEFPCM cavities. The results show how both the "position" of the distance-dependent decay (i.e., the separation for a chromophore pair at which $s \rightarrow 1$) and the final asymptotic value (s_0) for the solvent screening factor *s* differ for the $P_{D1}-P_{D2}$ dimer (∼face-to-face orientation, $s_0 = 0.57$) compared to the $Chl_{D1}-Ph_{D1}$ dimer (∼T-shape orientation, $s_0 = 0.61$). For both orientations, we find a similar decay of *s* as the D/A separation is enlarged, but the separation where $s = 1$ as well as the asymptotic screening are different. The origin of the exponential decay was analyzed in detail in our previous letter, using the $Chl_{602}-Chl_{607}$ pair of LHCII as an example.[49] We found it to be dictated by the process of forming a common cavity between D and A. The "shifting" of the decay profile could be a consequence of the different effective center-to-center distance at which each dimer occupies a common cavity in the medium as opposed to two separate ones. In the present example, however, both cavities merge at ∼18 Å and the shift in the decay is caused

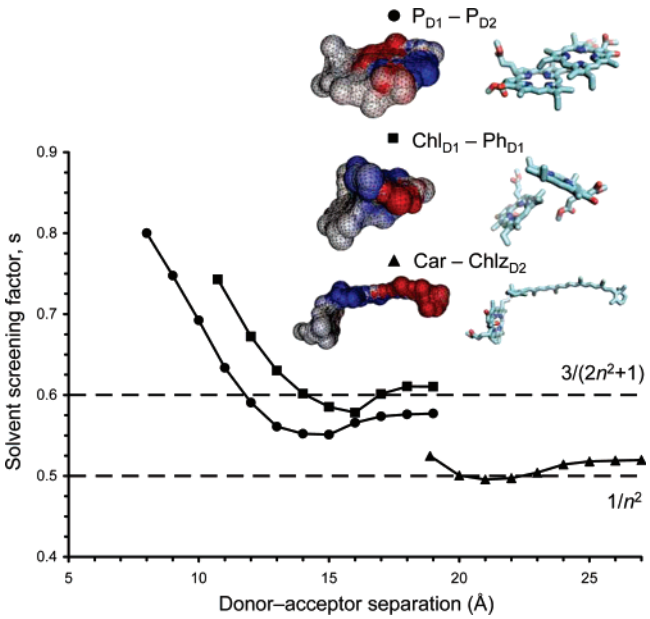

Figure 3. Distance-dependent screening profiles obtained for the $P_{D1}-P_{D2}$, $Chl_{D1}-Ph_{D1}$, and $Car-Chlz_{D2}$ dimers of PSII. The initial geometries taken from published structural models as well as the associated IEFPCM cavities are shown. Reaction potentials generated by the environment in response to ρ_D^T are represented on the cavity surface. Förster $1/n^2$ and Onsager $3/(2n^2 + 1)$ values are shown as horizontal lines.

TABLE 3: Distance-Dependent Profiles of V_s, $V_{explicit}$, and V for the $P_{D1}-P_{D2}$ Dimer Obtained by Changing the ϵ Value from 15 to 2, and the ϵ_{opt} Value from 2 to 10 (Couplings Are in cm^{-1})

(ϵ, ϵ_{opt})	(2,2)			(15,2)			(15,10)		
R (Å)	V_s	$V_{explicit}$	V	V_s	$V_{explicit}$	V	V_s	$V_{explicit}$	V
8	185	−36	149	181	−38	143	238	−106	132
9	150	−38	113	143	−37	106	192	−105	87
10	123	−38	85	116	−37	79	156	−100	56
11	101	−37	64	94	−35	59	129	−95	34
12	83	−34	48	77	−32	45	108	−87	21
13	68	−30	38	64	−28	36	91	−79	13
14	57	−26	31	54	−24	30	78	−69	10
15	48	−22	26	45	−20	25	67	−59	8
16	40	−18	23	38	−16	21	57	−50	7

instead by the different shape of dimer cavity formed during this merging process.

A significantly different behavior, however, is encountered for the $Car-Chlz_{D2}$ dimer ($s_0 = 0.52$). In this case, the environment of the chromophores (represented by their IEFPCM cavities) is not changed dramatically when a common cavity is formed at close separations. As a result, the $s = 0.52$ value at close separations equals the $s_0 = 0.52$ long-range value. In addition, in all three cases we observe a minimum on the s profiles. This subtle feature is a result of the different evolution of the $V_{explicit}$ term with respect to the V_s term as the cavities start to merge.

More interesting are the differences found for the asymptotic value of s. In fact, at close separations s has already been supposed to be dependent on the particular system, but at large donor−acceptor separations it is generally assumed to be constant, following Förster's $s_0 = 1/n^2$ value (for infinitely thin point dipoles) or Onsagers' $s_0 = 3/(2n^2 + 1)$ (for dipoles contained in spherical cavities). In our model of the screening, the use of molecular-shaped cavities leads to different s_0 values for each dimer. As shown in Figure 3, these estimates approximately range from Förster to Onsager predictions, and it is reasonable to think that real systems fall in between these two limits.

3.4. Dielectric Property Dependence. In the previous section, we have shown how the environment effect on EET coupling largely depends on the geometrical parameters of the interacting pigment pair. Obviously, even more important parameters determining such an effect are the dielectric properties of the environment itself. As described in the Methods, Section 2, the LR-IEFPCM approach requires two different dielectric permittivities to univocally determine the response of the environment to the EET, the static and the optical values. The static value is in fact the permittivity that determines the response of the environment to the ground-state unperturbed (and not interacting) chromophores while the optical value determines the response of the environment to the electronic transitions in the two chromophores and, even more importantly, screens the interaction that promotes energy transfer. It is thus easy to predict that the main effect on the EET coupling will be determined by the optical value (here equivalent to the square of the refractive index, see above) even if indirect effects due to a different description of the unperturbed systems owing to a change in the static permittivity passing, for example, from an apolar to a more polar environment can be significant.

As said above, to describe the dielectric properties of the environment (protein, intrinsic waters, and surrounding medium) around each chromophore we have selected the values of 2 for optical permittivity (ϵ_{opt}) and 15 for the static one (ϵ). Here, however, we test different values of both permittivities to quantify the dependence of the coupling on the dielectric properties of the medium; to this end, we have repeated the distance-dependent profiles of the $P_{D1}-P_{D2}$ dimer by changing the ϵ value from 15 to 2 and the ϵ_{opt} value from 2 to 10. We are aware that relevant materials for photosynthetic light harvesting have ϵ_{opt} values of about 2.5 as a maximum. However, we found it interesting to also test such high ϵ_{opt} values because of the growing number of applications of hybrid materials, for example involving semiconductor quantum dots or interfaces between organic materials and bulk semiconductors or metals.

In Table 3, we report the values of V_s, $V_{explicit}$, and V in the three different environments (the standard one, that with ϵ decreased to 2, and that with ϵ_{opt} increased to 10), and in Figure 4 the results are presented in a graphical form as screening factors.

As can be seen, by decreasing ϵ both V_s and $V_{explicit}$ decrease slightly leading to a small increase in the total coupling V. Such a trend is similar to that found by introducing ESP charges to mimic polarization effects of the other pigment in the pair (see Table 1). In general, however, the average effect of varying ϵ is less than 10%.

In contrast, if we increase the optical dielectric constant the changes are large: up to a 30% increase in V_s and a threefold change in $V_{explicit}$ can be noted in Table 3. This dramatic effect of ϵ_{opt} is exemplified graphically in Figure 4 where $s = (V_s + V_{explicit})/V_s$ is plotted for the three different environments together with the Förster and Onsager estimates. As expected, the screening is much greater in this environment, but an opposing significant enhancement of V_s is predicted for highly polarizable media. The most notable case is found for the closest separation (8 Å), where the total V coupling in the (15,10) medium is decreased only slightly (less than 10%) in comparison with the other dielectrics because the great increase in the screening is almost compensated by the implicit solvent effect.

TABLE 4: Donor−Acceptor (Center-to-Center) Separations, Orientation Factors, Screening Factors, and Electronic Couplings Obtained from the LR-IEFPCM Model and the PDA (Point-Dipole) Approximation for the Pigment Pairs of PSII and LHCII in Vacuum and in the Dielectric Medium (Couplings Are in cm^{-1})

			vacuum		dielectric				
	R (Å)	κ	V	V_{dd}	V_s	$V_{explicit}$	V	V_{dd}	s
PSII									
$Car-P_{D2}$	28.9	0.613	16	14	18	−8	10	8	0.54
$Car-Chl_{D2}$	18.3	0.436	39	41	39	−17	22	21	0.56
$Car-Chlz_{D2}$	18.9	0.696	104	55	118	−56	61	33	0.52
$Car-Ph_{D2}$	21.3	0.459	16	20	18	−9	10	12	0.52
$P_{D1}-P_{D2}$	8.0	0.856	147	244	181	−38	143	151	0.79
$P_{D1}-Chl_{D1}$	10.4	0.173	99	23	108	−32	76	10	0.71
$P_{D1}-Chl_{D2}$	12.2	1.586	120	133	148	−51	97	84	0.66
$P_{D1}-Ph_{D2}$	18.6	1.425	18	25	25	−11	14	17	0.56
$P_{D2}-Chl_{D1}$	12.1	1.527	99	132	123	−45	78	82	0.64
$P_{D2}-Chl_{D2}$	10.6	0.051	82	7	85	−23	62	−3	0.73
$P_{D2}-Ph_{D1}$	17.9	−1.594	−23	−32	−30	14	−17	−21	0.55
$Chl_{D1}-Chl_{D2}$	20.7	1.071	19	19	29	−11	18	14	0.61
$Chl_{D1}-Chlz_{D1}$	24.7	0.404	4	4	6	−2	3	3	0.61
$Chl_{D1}-Ph_{D1}$	10.7	0.930	101	87	127	−33	94	62	0.74
$Chl_{D1}-Ph_{D2}$	23.1	0.740	7	7	10	−4	6	5	0.60
$Chl_{D2}-Ph_{D1}$	22.8	−0.874	−9	−9	−13	5	−7	−6	0.59
$Chl_{D2}-Ph_{D2}$	10.9	−0.922	−93	−84	−119	32	−87	−60	0.73
$Chlz_{D1}-Ph_{D1}$	24.5	−0.750	−5	−6	−6	3	−4	−4	0.59
$Chlz_{D2}-Ph_{D2}$	23.4	−0.683	−5	−6	−6	3	−4	−4	0.58
$Ph_{D1}-Ph_{D2}$	21.1	−0.484	−5	−4	−7	3	−4	−3	0.58
LHCII									
$Chl_{602}-Chl_{607}$	9.8	1.595	355	332	416	−46	370	201	0.89

TABLE 5: Donor−Acceptor (Center-to-Center) Separations, Orientation Factors, Screening Factors, and Electronic Couplings Obtained from the LR-IEFPCM Model and the PDA (Point-Dipole) Approximation for the Pigment Pairs of PE545 in Vacuum and in the Dielectric Medium (Couplings Are in cm^{-1})

			vacuum		dielectric				
	R (Å)	κ	V	V_{dd}	V_s	$V_{explicit}$	V	V_{dd}	s
PEB′ 50/61C−PEB′ 50/61D	17.2	0.688	169	93	169	−77	92	49	0.54
PEB′ 50/61C−DBV 19B	25.3	−1.140	−64	−55	−68	31	−37	−29	0.54
PEB′ 50/61C−PEB 158C	25.7	0.877	39	36	42	−19	23	20	0.54
PEB′ 50/61C−PEB 158D	23.5	0.259	24	14	25	−13	12	7	0.48
PEB′ 50/61C−PEB 82C	24.2	0.871	66	44	70	−32	37	23	0.54
PEB′ 50/61C−PEB 82D	35.2	−1.197	−28	−20	−29	14	−16	−10	0.53
PEB′ 50/61D−DBV 19A	24.6	−1.135	−67	−57	−70	32	−39	−30	0.55
PEB′ 50/61D−PEB 158C	24.1	0.430	34	21	35	−17	18	11	0.51
PEB′ 50/61D−PEB 158D	25.3	0.977	43	41	46	−21	26	22	0.56
PEB′ 50/61D−PEB 82C	33.8	−1.200	−30	−22	−32	15	−17	−12	0.53
PEB′ 50/61D−PEB 82D	24.0	0.914	70	46	73	−33	40	24	0.55
DBV 19A−DBV 19B	43.2	−0.830	−7	−9	−8	3	−4	−5	0.58
DBV 19A−PEB 158C	22.3	0.381	63	27	63	−30	33	14	0.52
DBV 19A−PEB 82C	33.2	−1.033	−20	−22	−21	9	−11	−12	0.54
DBV 19A−PEB 82D	23.4	−1.485	−76	−90	−82	36	−46	−48	0.56
DBV 19B−PEB 158C	48.3	0.661	5	5	6	−3	3	2	0.52
DBV 19B−PEB 158D	21.8	0.320	65	24	65	−31	34	13	0.52
DBV 19B−PEB 82C	23.3	−1.420	−75	−90	−81	36	−45	−48	0.56
DBV 19B−PEB 82D	33.3	−1.049	−20	−23	−21	10	−11	−12	0.54
PEB 158C−PEB 158D	45.6	1.041	10	8	10	−5	6	4	0.55
PEB 158C−PEB 82C	38.8	−0.720	−12	−9	−13	6	−7	−5	0.52
PEB 158C−PEB 82D	39.9	0.962	13	11	13	−6	7	6	0.54
PEB 158D−PEB 82C	38.8	0.772	10	9	11	−5	6	5	0.54
PEB 158D−PEB 82D	38.7	−0.775	−13	−10	−14	7	−7	−5	0.52
PEB 82C−PEB 82D	35.9	−0.391	−6	−6	−6	3	−3	−3	0.53

Besides the variation in "position" and asymptotic screening values calculated for the environments with different ϵ_{opt}, we note the different exponential decays. When a larger ϵ_{opt} is used, the screening increases (i.e., s decreases) more rapidly with distance showing that the error introduced by the use of a constant screening factor can depend significantly on the polarizability of the environment.

All of the analyses presented in these three sections focused on three selected pairs are finally reconsidered and generalized for the full set of over 100 pairs (note that we plot less than 100 because we choose only the couplings greater than 5 cm^{-1}) of molecules in four different photosynthetic proteins in the following section.

3.5. EET Coupling in Photosynthetic Systems. In this section, we analyze the practical implications of three common assumptions used in the modeling of EET phenomena in photosynthetic light-harvesting systems, namely (i) the use of simple Förster's screening factor $s = 1/n^2$, (ii) the neglect of the change in the properties of the chromophores upon passage from vacuum to a condensed phase environment, and (iii) the use of the point-dipole approximation. This analysis is based on the electronic couplings obtained with the LR-IEFPCM

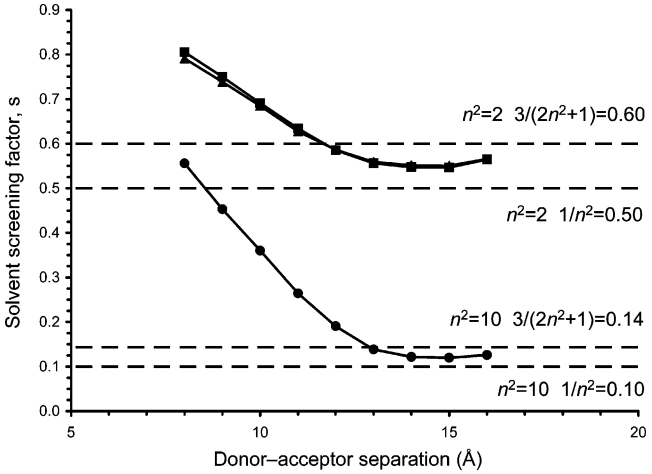

Figure 4. Distance-dependent screening profiles obtained for the $P_{D1}-P_{D2}$ dimer of PSII obtained in different dielectric environments. Data correspond to $\epsilon = 2/\epsilon_{opt} = 2$ (squares), $\epsilon = 15/\epsilon_{opt} = 2$ (triangles), and $\epsilon = 15/\epsilon_{opt} = 10$ (circles). Förster $1/\epsilon_{opt}$ and Onsager $3/(2\epsilon_{opt} + 1)$ values are shown for ϵ_{opt} values 10 and 2 as horizontal lines.

model both in vacuum and with inclusion of medium effects for the series of pigment pairs considered. We note that in order to avoid numerical inaccuracies the final data set is defined by considering only pairs having V_s couplings larger than 5 cm^{-1}. For the present analysis, it will be useful to introduce the popular point-dipole approximation (PDA) adopted in Förster theory, in which the electronic coupling is given by

$$V = sV_s \approx sV_{dd} = \frac{1}{n^2}\frac{\kappa \mu_D^T \mu_A^T}{R^3} \quad (8)$$

where the orientation factor is $\kappa = \hat{\mu}_D^T \cdot \hat{\mu}_A^T - 3(\hat{\mu}_D^T \cdot \hat{R})(\hat{\mu}_A^T \cdot \hat{R})$ and μ_D^T/μ_A^T are transition dipole moments of donor and acceptor molecules separated by a distance R ($\hat{\mu}_D^T$, $\hat{\mu}_A^T$, and $\hat{R}$ are the corresponding unit vectors).

3.5.1. Dielectric Effects. In our previous letter, we reported a distance-dependent screening for the present data set.[49] The s function introduced in that work, obtained by fitting the results and therefore averaged over multiple chromophores, shapes, and orientations, is given by

$$s = A \exp(-\beta R) + s_0 \quad (9)$$

where the pre-exponential factor is $A = 2.68$, the attenuation factor is $\beta = 0.27$, and $s_0 = 0.54$ is the asymptotic value of s at large distances. This empirical screening function indicates that $s = 1$ at an interchromophoric (center-to-center) separation $R = 6.6$ Å, and the expression is valid for distances larger than this value.

The introduction of a distance-dependent s function significantly improves the predictions of electronic couplings over that obtained by assuming a constant s factor. For instance, a least mean-square fit $V = s \cdot V_s$ between V_s and V couplings obtained in the dielectric medium leads to an averaged $s = 0.68$ value. This fixed s factor leads to a MUE (mean unsigned error) of 7 cm^{-1} in the estimation of V, whereas the predictions based on eq 9 lead to a lower MUE value of 3 cm^{-1}. Because of the range of computed couplings (from a few units to more than 300 cm^{-1}), a better estimate of the predictive power is given by the MPUE (mean percent unsigned error), equal to 4% by using the distance-dependent s function compared to the much larger 23% average error obtained with the constant factor.

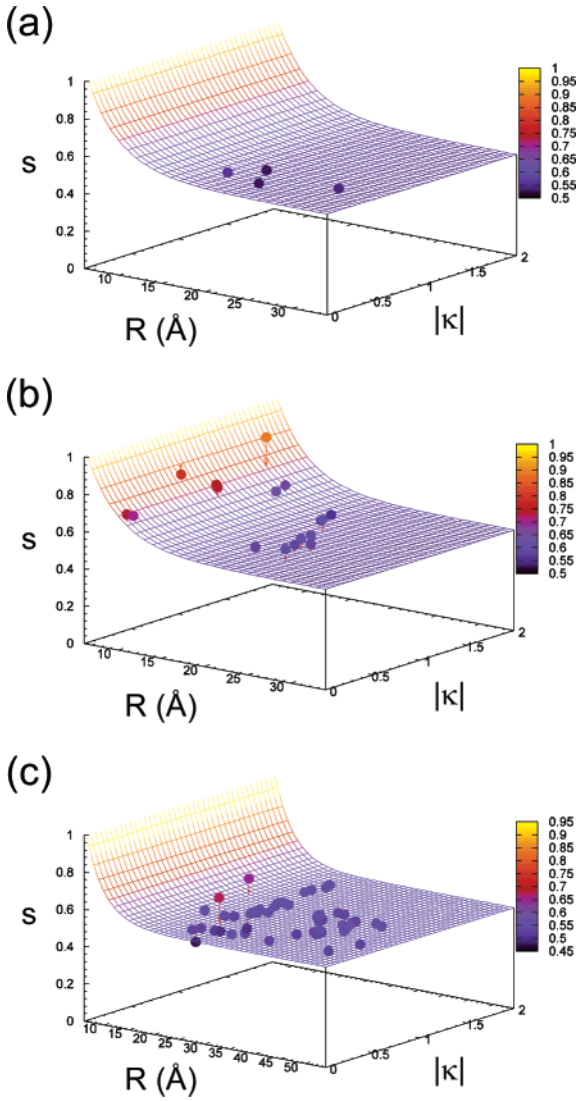

Figure 5. Screening factor s represented as a function of the donor–acceptor separation R and the absolute value of the orientation factor $|\kappa|$. The surface represents the s function defined in eq 9, and data points correspond to (a) pairs involving the carotenoid in PSII, (b) other pairs from PSII and LHCII, and (c) pairs from PE545 and PC645. Red arrows connecting the points to the corresponding predictions on the surface are shown to facilitate visualization.

It is interesting to compare this average $s = 0.68$ estimate to the value $s = 0.80$ obtained by Adolphs and Renger[41] for the chromophores of the Fenna–Matthews–Olson (FMO) complex. In that study, electronic couplings were obtained from atomic transition monopole (TM) charges, and the effect of the environment was introduced by numerically solving the Poisson equation by a finite difference method, a popular approach used in electrostatic calculations of biomolecules. Their larger $s = 0.80$ factor can be explained noting that in the FMO complex chromophores are more closely packed and their analysis is focused on the effect of the protein on the coupling, while they do not consider the polarizing effect exerted by the rest of the chromophores or by intrinsic/surrounding waters.

As illustrated in Section 3.3, the precise value of s depends on the shape, orientation, and separation between the chromophores. In Tables 4 and 5, we report the screening factors and the couplings obtained for PSII/LHCII and PE545, respectively, both in vacuum and in the dielectric medium (the results for PC645 are analogous to those obtained for PE545 and are not shown), and in Figure 5 we show the screening factors

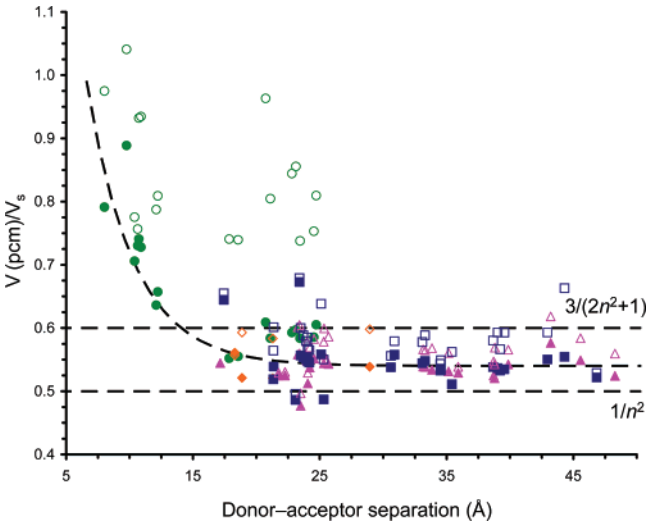

Figure 6. V/V_s ratios calculated from V couplings computed in the medium and V_s terms obtained in vacuum (empty symbols) and in the medium (filled symbols). Data points correspond to the following: pink triangles = PE545, blue squares = PC645, green circles = PSII or LHCII, except orange diamonds = data involving the carotenoid in PSII. Förster $1/n^2$ and Onsager $3/(2n^2 + 1)$ values are shown as horizontal lines, and the curve represents the fitted screening function defined by eq 9.

obtained for the data set as a function of R and the absolute value of the orientation factor $|\kappa|$, along with the surface defined by eq 9.

Figure 5 illustrates the wide range of orientations explored in this analysis, especially for pigment pairs involving chlorophylls and bilins, shown in plots b and c, respectively. At large donor−acceptor separations, the s values are found to be quite constant along the data set. In contrast, at short distances the precise value of s is more dependent on the particular shape and orientation of the pigment pair considered. For the closest chlorophyll pairs shown, in fact, a trend is observed in which s decreases passing to smaller values of $|\kappa|$. However, the overall agreement between the points and the averaged s function is good for the entire range of distances and orientations explored.

As already discussed in Section 3.3, the possibility that the long-range s_0 value can change for different systems is in general not recognized. In our calculations, s reaches an averaged asymptotic $s_0 = 0.54$ value at large distances. This result is intermediate between the limiting cases of screening between (infinitely thin) point dipoles, $s_0 \approx 1/n^2 = 0.5$ (as assumed in Förster model) and the prediction of Onsager theory, which considers two dipoles inserted in *spherical* cavities, $s_0 \approx 3/(2n^2 + 1) = 0.6$. It is reasonable that real molecules fall somewhere between the limits of Förster and Onsager limits, as dictated by their shapes.

We turn now our analysis on the evaluation of implicit solvation effects on the coupling, that is, those induced by the change in the transition densities of the chromophores upon passage from the gas phase to a particular condensed phase environment. The variation of the transition density (or dipole) upon solvation can be very different depending on the characteristics of the particular chromophore and electronic excitation under study.

For the pigments considered here, a much greater change in the transition dipole in the polarizable medium compared to vacuum is calculated for chlorophyll-*a* (∼15%) and pheophytin-*a* (∼22%) than for the carotenoid β-carotene (∼0%) and bilins (∼2−7%). The significant enhancements thus induced on V_s (see Tables 4 and 5) mean that not only a correct description of screening effects but also an account of the changes in the transition densities upon solvation is needed in order to obtain good estimates of electronic coupling. However, because the enhancement of V_s greatly depends on the particular pair under examination, it is not possible to define an averaged empirical expression for this implicit solvent effect as the one we report for the screening. This fact is illustrated in Figure 6, where we show the V/V_s ratios calculated from the total couplings obtained in the medium and the V_s terms computed either in vacuum or in the medium (in the latter case the previously defined s screening factor). It can be seen that it is not possible to define a scaling function to be applied to the vacuum V_s values in order to reproduce the total electronic couplings in condensed phase. This would be possible only if no implicit solvent effects were present; in that case, it would coincide with s.

At this point, it is worth mentioning a practical strategy used in the calculation of electronic couplings that consists of scaling the transition densities (or dipoles) obtained in the gas phase in order to reproduce the transition dipoles observed experimentally.[13,31] This scaling enables correction for inaccuracies in the quantum-mechanical level of theory adopted and also introduces implicit solvation effects in some way. However, caution must be taken in applying this procedure because the change induced in the transition properties upon solvation can be more complex than a simple scalar variation of the transition dipole. In addition, the transition dipole of a chromophore can be quite different depending on the particular environment and conformation. For instance, we found a variation of ∼8% between the transition dipole of chlorophyll-*a* in Chl_{D2} (6.6 D) and $Chlz_{D2}$ (6.1 D) that would be neglected if both were scaled to reproduce a common value. Here, no scaling has been attempted because the present report is not focused on the precise value of the couplings but rather on the factors affecting its estimation. Nevertheless, we have included as Supporting Information the transition dipoles and energies obtained in the calculations so that other researchers could perform such a scaling.

3.5.2. Comparison with the Point-Dipole Approximation. It is interesting to also comment on the consequences arising from the adoption of the popular point-dipole approximation (PDA) to estimate electronic couplings. This issue has been widely discussed in the literature, and it is clear that the PDA fails when the interchromophoric distance is smaller than the dimensions of the interacting chromophores because in this range the shape of the molecules becomes very important.[1] In Figure 7, we show the ratio between the direct V_s couplings obtained in the medium and the PDA couplings V_{dd}, eq 8, obtained from the transition dipoles of the corresponding LR-IEFPCM calculations. As expected, the agreement between both is increased gradually with larger interchromophore separations. However, even at distances much larger than the dimensions of the pigments considered (∼15 Å for chlorophylls and bilins, ∼27 Å for β-carotene) we found significant deviations.

For chlorophyll-type macrocycle pairs with separations larger than 15 Å, we find a MPUE (mean percent unsigned error) between V_s and V_{dd} of 16%. Three of those pairs are found to have absolute errors over 20%: $P_{D1}-Ph_{D2}$ (35%), $P_{D2}-Ph_{D1}$ (41%), and $Chlz_{D2}-Ph_{D2}$ (24%). Alternatively, the bilin pairs are separated by distances larger than the dimension of each chromophore, yet the MPUE found amounts to 26%. Moreover, at separations larger than 30 Å the errors are still significant, and the MPUE is only reduced to 23%. A very extensive comparison between the couplings obtained from the PDA and the transition density cube (TDC) method for the pigments of

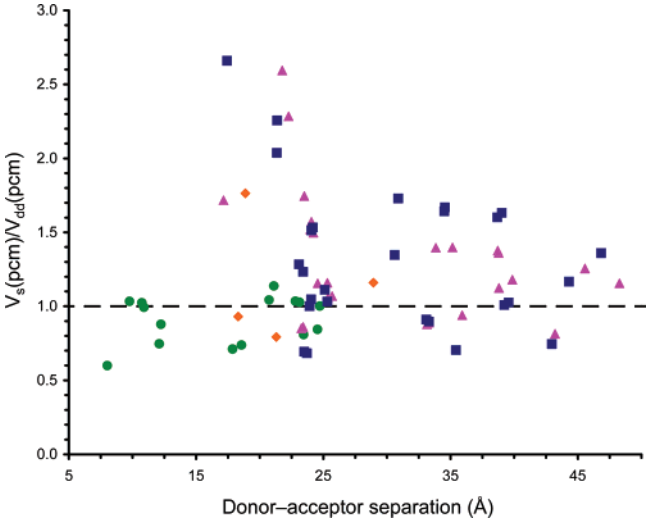

Figure 7. Ratio between V_s and V_{dd} PDA couplings (estimated from the transition dipoles as obtained from the corresponding LR-IEFPCM calculations) represented as a function of the donor−acceptor (center-to-center) distance. Data points correspond to the following: pink triangles = PE545, blue squares = PC645, green circles = PSII or LHCII, except orange diamonds = data involving the carotenoid in PSII.

LHCII has been published recently.[70] The conclusions of that study are similar to ours: the PDA can be significantly in error for closely packed photosynthetic pigment pairs at distances less than 25 Å. In addition, our results show that for photosynthetic proteins having bilin chromophores deviations can be significant at even larger distances, probably owing to their elongated and somewhat asymmetric structure.

3.5.3. Implications for Quantitative Models of EET. Finally, we illustrate the consequences of our analysis on some quantitative models of EET, such as those actively pursued in the study of photosynthetic light-harvesting systems.

In photosynthetic antenna and reaction centers, nearest-neighbor separations between light-harvesting molecules range typically from 8 to 11 Å. One notable exception, though, is phycobiliproteins, such as PE545 and PC645, wherein average nearest-neighbor chromophore separations are ∼17 Å. It can be expected then that key interchromophoric interactions in such systems occur at separations approximately ranging from 8 to 20 Å, thus falling in the region where our fitted screening function shows an exponential decay. Our observation of a distance-dependent screening can thus potentially improve the agreement between theory and experiment in such models and also explain the variety of ϵ_{opt} values often adopted because it is common to simultaneously fit ϵ_{opt} and the transition dipole magnitudes of the pigments in order to reproduce experimental spectroscopic data using the point-dipole approximation (PDA) along with Förster $s = 1/\epsilon_{opt}$ screening factor. For example, such fitting procedures gave ϵ_{opt} values in the range of 1.2−1.5 in the modeling of light-harvesting complexes 1 (LH1) and 2 (LH2) from purple bacteria,[71,72] values that are probably too low for a protein environment.

A more satisfactory picture appears by considering the screening function, eq 9, which gives screenings corresponding to ϵ_{opt} values in the range of 1.2−1.5 over the distance range 8−11 Å while using $\epsilon_{opt} = 2$. The spectroscopic features of such complexes are known to be particularly dependent on a proper description of the interactions between the most strongly coupled chromophores.[73] Now that more detailed structural models are available for an increasing variety of light-harvesting antenna proteins, a better model for screening of electronic interactions will aid, and in turn be tested by, simulation of various electronic spectra as well as prediction of energy migration dynamics.

Another example of the implications of our analysis can be drawn for a recent study by Jang and co-workers.[74] In this case, the BChl-Q_Y transition dipole was estimated to be 6.5−7.5 D by assuming ϵ_{opt} values in the range of 1.5−2 when reproducing the multichromophoric energy transfer times between the B800 and B850 units of LH2. In this system, typical interpigment separations are ∼9 Å (B850−B850 interactions) and ∼18 Å (B800−B850 interactions). These distances give screening factors in the range of 0.56−0.78 for an $\epsilon_{opt} = 2$ value from our *s* function, screenings that would lead to a new estimated dipole in the 6.0−7.1 D range, in good accord with the 6.1 D result predicted by the empty cavity analysis reported by Knox and Spring.[75] Interestingly, it is not clear whether refinement of the screening would lead to an increased or decreased B800−B850 energy transfer time. This is because the *s* function could lead to either an enlarged coupling (and therefore exciton delocalization) inside the B850 ring or alternatively to a weakened (more screened) interaction between the B850 and the B800 chlorophylls.[39]

4. Summary

In the present work, we have analyzed the key implications of dielectric effects on EET couplings in photosynthetic antenna proteins. A recently developed quantum-mechanical model, that combines a linear response approach with the IEFPCM solvation model, was applied to examine the screening and the implicit solvent effect on transition densities. This methodology captures the key features of the problem, such as an accurate calculation of excited states, the shape of molecules, and the response of the surrounding medium to charge and, importantly, transition densities.

We showed that although the quantum-mechanical level of description can affect the magnitude of the coupling values, the screening of EET interactions, as given by the *s* factor, is found to be quite insensitive to the quantum-mechanical treatment. In contrast, the precise value of the screening is greatly dependent on the geometrical details (distance, shape, and orientation) of the chromophore pair considered. In particular, screening effects are greatly reduced at close interchromophore separations as a result of the exclusion of the host medium in the intermolecular region. In addition, we showed that implicit as well as explicit medium effects, these latter estimated by the screening factor *s*, are dictated mainly by the optical dielectric properties of the medium (ϵ_{opt}), while the effect of the static properties (ϵ) is substantially less important.

By analyzing over 100 pairs of chromophores taken from different photosynthetic light-harvesting antenna proteins, we showed how the definition of an empirical distance-dependent screening function, averaged over different shapes and orientations, greatly improves the predictions of electronic coupling in such systems over the simple Förster screening factor of $1/n^2$. Typical nearest-neighbor separations between light-harvesting molecules range from 8 to 11 Å. Therefore, the empirical expression we obtained, eq 9, has significant implications for the development of more accurate quantitative models of EET and light-harvesting dynamics in photosynthetic systems because we discovered that the screening depends significantly on the interchromophore separation over this distance range. Using the empirical expression means that other workers do not need to calculate explicitly medium effects for the kinds of chro-

mophores we have considered. In addition, this finding can potentially help in reconciliating the variety of effective ϵ_{opt} values estimated from such models for different light-harvesting antenna proteins.

We conclude that the close packing between chromophores observed in many natural antenna systems leads to a situation where medium screening effects are reduced significantly, enabling more efficient energy migration and trapping than would otherwise be predicted. This result should be considered in the design of artificial light-harvesting devices for the capture and transfer of electronic excitation.

Appendix

A1. Reaction Field of a Nonpolarizable Point Dipole. Let us consider an unpolarized medium of dielectric constant ϵ and introduce a rigid dipole of moment m into a spherical cavity of radius a.

The potential ψ has to satisfy Laplace's equation and the boundary conditions.

The solution of the problem is (in polar coordinates)

$$\psi(r, \theta; r < a) = \psi^{in} = \frac{m \cos\theta}{r^2} - Rr\cos\theta \qquad (A1)$$

$$\psi(r, \theta; r > a) = \psi^{out} = \frac{m^* \cos\theta}{\epsilon r^2} \qquad (A2)$$

where

$$m^* = \frac{3\epsilon}{2\epsilon + 1} m \qquad (A3)$$

$$R = \frac{2(\epsilon - 1)}{2\epsilon + 1}\frac{m}{a^3} = f^R m \qquad (A4)$$

R is called the "reaction field"; it measures the electric field that acts upon the dipole as a result of electric displacements induced by its own presence.

m^* is called the "external moment" of the immersed dipole; it determines the force (modified by the interventing medium) that the dipole will exert upon a distant charge in the dielectric.

As a result, the interaction energy between the dipole and such a distant charge in the dielectric becomes

$$\psi^{out}(r, \theta)\, q(r) = \frac{m^* \cos\theta}{\epsilon r^2} q = \frac{3\epsilon}{2\epsilon + 1} m \frac{\cos\theta}{\epsilon r^2} q = \frac{3}{2\epsilon + 1}\psi^0(r, \theta) q \qquad (A5)$$

where $\psi^0(r, \theta)$ is the potential produced by the dipole in vacuo. This is the expression of the interaction energy in vacuo modified by the dielectric through the factor

$$s^O = \frac{3}{2\epsilon + 1} \qquad (A6)$$

s^O can be defined as an *effective screening factor*.

Hsu et al.[25] showed that the expression for the EET coupling is isomorphic to the interaction of two electronic densities (or dipoles) under the influence of a dielectric medium except that in EET the transition densities (or dipoles) for the donor and acceptor and the dynamic dielectric properties at the frequency of the transition have to be used. In that work, the Onsager effective screening factor of eq A6 was derived for EET. In this context, the Förster $1/\epsilon$ screening factor is the corresponding expression to eq A6 if the cavity is neglected and the point dipole is immersed directly in the dielectric.

This theory can be translated in the notation used by Knox and Amerongen[26] introducing two different permittivities, $\epsilon_{(1)} = n^2_{(1)}$ and $\epsilon_{(2)} = n^2_{(2)}$, for the external potential ψ^{out} and external dipole m^* (which now becomes the in situ dipole moment), respectively

$$m^* = \mu(n_{(2)}) = \frac{3n^2_{(2)}}{2n^2_{(2)} + 1} m \qquad (A7)$$

$$\psi^{out} = \frac{\mu(n_{(2)}) \cos\theta}{n^2_{(1)} r^2} \qquad (A8)$$

while the effective screening factor should read

$$s^O = \frac{1}{\epsilon_{(1)}}\frac{3\epsilon_{(2)}}{2\epsilon_{(2)} + 1} \qquad (A9)$$

We note that eqs A6 or A9 should be applied along with the "vacuum" transition moments m instead of the in situ dipoles m^* discussed by Knox and Amerongen in order to obtain the coupling. However, as will be discussed in next section, these "vacuum" dipoles are polarizable so they will also be affected by the environment.

A2. Reaction Field of a Polarizable Point Dipole. In this case, the reaction field R induces a dipole αR

$$R = f^R(m^0 + \alpha R) \qquad (A10)$$

where m^0 is the permanent dipole moment (let us say the vacuum value) and α its polarizability. Therefore

$$R = \frac{f^R}{1 - f^R\alpha} m^0 \qquad (A11)$$

Under the influence of this reaction field, the dipole moment is increased:

$$m^{sol} = m^0 + \alpha R = \frac{m^0}{1 - f^R\alpha} = \frac{m^0}{1 - \frac{\alpha}{a^3}\frac{2(\epsilon - 1)}{2\epsilon + 1}} \qquad (A12)$$

Also in this case we can define an external dipole moment

$$m^* = \frac{3\epsilon}{2\epsilon + 1} m^{sol} \qquad (A13)$$

and an effective screening factor s^O exactly as before.

A3. Implicit versus Explicit Contributions. In PCM, the reaction field R is represented in terms of an apparent surface charge: this approach allows us to extend the Onsager approach to any kind of molecular shape (not just a sphere or an ellipse) and any kind of charge distribution (not only a dipole).

As for the Onsager model (see eqs A4 and A11), R^{PCM} will depend on the dielectric constant ϵ, the cavity shape, and the solute charge distribution, which in general will be polarizable. The presence of this reaction field will modify all of the properties of the solute, including its dipole moment, which will be increased exactly as it happens in the Onsager model (see eq A12).

By applying these considerations to EET coupling, we have to consider that the interacting bodies are transition densities. These will be modified by the solvent reaction field R^{PCM} exactly

as the normal dipole moment in the polarizable case (by simplifying $\mu_{A,D}^{T,sol} = \mu_{A,D}^{T,0} + \alpha_{A,D}^{T} R^{PCM}$).

By considering only this effect, the EET coupling would be modified because the transition densities have been modified with respect to the in vacuo case. This is what we call **implicit** contribution, that is, (neglecting exchange effects):

$$V_s = \int d\mathbf{r} \int d\mathbf{r}' \rho_A^{T,sol*}(\mathbf{r}') \frac{1}{|\mathbf{r}' - \mathbf{r}|} \rho_D^{T,sol}(\mathbf{r}) \neq \int d\mathbf{r} \int d\mathbf{r}' \rho_A^{T,0*}(\mathbf{r}') \frac{1}{|\mathbf{r}' - \mathbf{r}|} \rho_D^{T,0}(\mathbf{r}) \quad \text{(A14)}$$

In addition to that, however, we have to consider the equivalent of what is reported in eq A5. In PCM, this **explicit** effect is accounted for by calculating the interaction energy between the apparent charges induced by the donor transition density and the acceptor transition density (see eq 6 with $\epsilon_\omega = n^2$ and $\rho_X^T = \rho_X^{T,sol}$). In our model, we do not make distinction between $\epsilon_{(1)} = n_{(1)}^2$ and $\epsilon_{(2)} = n_{(2)}^2$.

Finally, the total coupling is the sum of the two terms (see eq 4) and the *s* factor defined in eq 7 is the equivalent of the Onsager effective screening factor.

Acknowledgment. G.D.S. acknowledges the support of the Natural Sciences and Engineering Research Council of Canada and an E. W. R. Steacie Memorial Fellowship. C.C., B.M., and R.C. acknowledge the financial support of the Italian "Ministero dell'Università e Ricerca" (PRIN 2005).

Supporting Information Available: Transition dipoles and energies in vacuum and in the dielectric environment obtained from CIS/6-31G calculations for the chromophores of PSII, LHCII, and PE545. This material is available free of charge via the Internet at http://pubs.acs.org.

References and Notes

(1) Scholes, G. D. *Annu. Rev. Phys. Chem.* **2003**, *54*, 57.
(2) Swager, T. M. *Acc. Chem. Res.* **1998**, *31*, 201.
(3) Brédas, J. L.; Beljonne, D.; Coropceanu, V.; Cornil, J. *Chem. Rev.* **2004**, *104*, 4971.
(4) Jares-Erijman, E.; Jovin, T. M. *Nat. Biotechnol.* **2003**, *21*, 1387.
(5) Lippincott-Schwartz, J.; Snapp, E.; Kenworthy, A. *Nat. Rev. Struct. Biol.* **2001**, *2*, 444.
(6) Weiss, S. *Nat. Struct. Biol.* **2000**, *7*, 724.
(7) Fleming, G. R.; Scholes, G. D. *Nature* **2004**, *431*, 256.
(8) Sündstrom, V.; Pullerits, T.; van Grondelle, R. *J. Phys. Chem. B* **1999**, *103*, 2327.
(9) van Grondelle, R.; Dekker, J. P.; Gillbro, T.; Sündstrom, V. *Biochim. Biophys. Acta* **1994**, *1187*, 1.
(10) van Amerongen, H.; Valkunas, L.; van Grondelle, R. *Photosynthetic Excitons*; World Scientific Publishers: Singapore, 2000.
(11) Melkozernov, A. N.; Barber, J.; Blankenship, R. E. *Biochemistry* **2006**, *45*, 331.
(12) Cogdell, R. J.; Gall, A.; Kohler, J. *Q. Rev. Biophys.* **2006**, *39*, 227.
(13) Scholes, G. D.; Fleming, G. R. *Adv. Chem. Phys.* **2005**, *132*, 57.
(14) Gust, D.; Moore, T. A.; Moore, A. L. *Acc. Chem. Res.* **2001**, *34*, 40.
(15) Jolliffe, K. A.; Bell, T. D. M.; Ghiggino, K. P.; Langford, S. J.; Paddon-Row, M. N. *Angew. Chem., Int. Ed.* **1998**, *37*, 915.
(16) Berera, R.; Herrero, C.; van Stokkum, I. H. M.; Vengris, M.; Kodis, G.; Palacios, R. E.; van Amerongen, H.; van Grondelle, R.; Gust, D.; Moore, T. A.; Moore, A. L.; Kennis, J. T. M. *Proc. Natl. Acad. Sci. U.S.A.* **2006**, *103*, 5343.
(17) Balzani, V.; Campagna, S.; Denti, G.; Juris, A.; Serroni, S.; Venturi, M. *Acc. Chem. Res.* **1998**, *31*, 26.
(18) Holten, D.; Bocian, D. F.; Lindsey, J. S. *Acc. Chem. Res.* **2002**, *35*, 57.
(19) Förster, T. *Ann. Phys.* **1948**, *2*, 55.
(20) Scholes, G. D.; Ghiggino, K. P. *J. Phys. Chem.* **1994**, *98*, 4580.
(21) van Grondelle, R.; Novoderezhkin, V. I. *Phys. Chem. Chem. Phys.* **2006**, *8*, 793.
(22) Jang, S.; Newton, M. D.; Silbey, R. J. *Phys. Rev. Lett.* **2004**, *92*, 218301.
(23) Lee, H.; Cheng, Y.-C.; Fleming, G. R. *Science* **2007**, *316*, 1462.
(24) Engel, G. S.; Calhoun, T. R.; Read, E. L.; Ahn, T.-K.; Mančal, T.; Cheng, Y.-C.; Blankenship, R. E.; Fleming, G. R. *Nature* **2007**, *446*, 782.
(25) Hsu, C.-P.; Fleming, G. R.; Head-Gordon, M.; Head-Gordon, T. *J. Chem. Phys.* **2001**, *114*, 3065.
(26) (a) Knox, R. S.; van Amerongen, H. *J. Phys. Chem. B* **2002**, *106*, 5289. (b) Knox, R. S. *Photochem. Photobiol.* **2003**, *77*, 492.
(27) Iozzi, M. F.; Mennucci, B.; Tomasi, J.; Cammi, R. *J. Chem. Phys.* **2004**, *120*, 7029.
(28) Agranovich, V. M.: Galanin, M. D. *Electronic Excitation Energy Transfer in Condensed Matter*; North-Holland: Amsterdam, 1982.
(29) (a) Juzeliūnas, G.; Andrews, D. L. *Phys. Rev. B* **1994**, *49*, 8751. (b) Juzeliūnas, G.; Andrews, D. L. *Phys. Rev. B* **1994**, *50*, 13371. (c) Juzeliūnas, G.; Andrews, D. L. *J. Lumin.* **1994**, *60/61*, 834.
(30) Dow, J. D. *Phys. Rev.* **1968**, *174*, 962.
(31) Krueger, B. P.; Scholes, G. D.; Fleming, G. R. *J. Phys. Chem. B* **1998**, *102*, 5378.
(32) Wong, K. F.; Bagchi, B.; Rossky, P. J. *J. Phys. Chem. A* **2004**, *108*, 5752.
(33) Beljonne, D.; Pourtois, G.; Silva, C.; Hennebicq, E.; Herz, L. M.; Friend, R. H.; Scholes, G. D.; Setayesh, S.; Müllen, K.; Brédas, J. L. *Proc. Natl. Acad. Sci. U.S.A.* **2002**, *99*, 10982.
(34) Beenken, W. J. D.; Pullerits, T. *J. Chem. Phys.* **2004**, *120*, 2490.
(35) Beljonne, D.; Cornil, J.; Silbey, R.; Millie, P.; Bredas, J. L. *J. Chem. Phys.* **2000**, *112*, 4749.
(36) Madjet, M. E.; Abdurahman, A.; Renger, T. *J. Phys. Chem. B* **2006**, *110*, 17268.
(37) Orozco, M.; Luque, F. J. *Chem. Rev.* **2000**, *100*, 4187.
(38) (a) Tretiak, S.; Middleton, C.; Chernyak, V.; Mukamel, S. *J. Phys. Chem. B* **2000**, *104*, 4519. (b) Tretiak, S.; Middleton, C.; Chernyak, V.; Mukamel, S. *J. Phys. Chem. B* **2000**, *104*, 9540.
(39) Scholes, G. D.; Fleming, G. R. *J. Phys. Chem. B* **2000**, *104*, 1854.
(40) Cory, M. G.; Zerner, M. C.; Hu, X.; Schulten, K. *J. Phys. Chem. B* **1998**, *102*, 7640.
(41) Adolphs, J.; Renger, T. *Biophys. J.* **2006**, *91*, 2778.
(42) Cohen, B. E.; McAnaney, T. B.; Park, E. S.; Jan, Y. N.; Boxer, S. G.; Jan, L. Y. *Science* **2002**, *296*, 1700.
(43) Golosov, A. A.; Karplus, M. *J. Phys. Chem. B* **2007**, *111*, 1482.
(44) King, G.; Lee, F. S.; Warshel, A. *J. Chem. Phys.* **1991**, *95*, 4366.
(45) Smith, P. E.; Brunne, R. M.; Mark, A. E.; van Gunsteren, W. F. *J. Phys. Chem.* **1993**, *97*, 2009.
(46) Pitera, J. W.; Falta, M.; van Gunsteren, W. F. *Biophys. J.* **2001**, *80*, 2546.
(47) Simonson, T.; Brooks, C. L. *J. Am. Chem. Soc.* **1996**, *118*, 8452.
(48) Curutchet, C.; Mennucci, B. *J. Am. Chem. Soc.* **2005**, *127*, 16733.
(49) Scholes, G. D.; Curutchet, C.; Mennucci, B.; Cammi, R.; Tomasi, J. *J. Phys. Chem. B* **2007**, *111*, 6978.
(50) Hennebicq, E.; Pourtois, G.; Scholes, G. D.; Herz, L. M.; Russell, D. M.; Silva, C.; Setayesh, S.; Grimsdale, A. C.; Mullen, K.; Bredas, J.-L.; Beljonne, D. *J. Am. Chem. Soc.* **2005**, *127*, 4744.
(51) (a) Cancès, E.; Mennucci, B. *J. Math. Chem.* **1998**, *23*, 309. (b) Cancès, E.; Mennucci, B.; Tomasi, J. *J. Chem. Phys.* **1997**, *107*, 3031. (c) Mennucci, B.; Cancès, E.; Tomasi, J. *J. Phys. Chem. B* **1997**, *101*, 10506.
(52) (a) Miertus, S.; Scrocco, E.; Tomasi, *J. Chem. Phys.* **1981**, *55*, 117. (b) Cammi, R.; Tomasi, J. *J. Comput. Chem.* **1995**, *16*, 1449.
(53) Tomasi, J.; Persico, M. *Chem. Rev.* **1994**, *94*, 2027.
(54) Tomasi, J.; Mennucci, B.; Cammi, R. *Chem. Rev.* **2005**, *105*, 2999.
(55) (a) Cammi, R.; Mennucci, B. *J. Chem. Phys.* **1999**, *110*, 9877. (b) Cammi, R.; Mennucci, B.; Tomasi, J. *J. Phys. Chem. A* **2000**, *104*, 5631.
(56) Russo, V.; Curutchet, C.; Mennucci, B. *J. Phys. Chem. B* **2007**, *111*, 853.
(57) Curutchet, C.; Cammi, R.; Mennucci, B.; Corni, S. *J. Chem. Phys.* **2006**, *125*, 054710.
(58) Mennucci, B.; Tomasi, J.; Cammi, R. *Phys. Rev. B* **2004**, *70*, 205212.
(59) Magyar, R. J.; Tretiak, S. *J. Chem. Theory Comput.* **2007**, *3*, 976.
(60) Loll, B.; Kern, J.; Saenger, W.; Zouni, A.; Biesiadka, J. *Nature* **2005**, *438*, 1040.
(61) Doust, A. B.; Wilk, K. E.; Curmi, P. M. G.; Scholes, G. D. *J. Photochem. Photobiol., A* **2006**, *184*, 1.
(62) Standfuss, J.; Terwisscha van Scheltinga, A. C.; Lamborghini, M.; Kühlbrandt, W. *EMBO J.* **2005**, *24*, 919.
(63) Frisch, M. J.; Trucks, G. W.; Schlegel, H. B.; Scuseria, G. E.; Robb, M. A.; Cheeseman, J. R.; Montgomery, J. A., Jr.; Vreven, T.; Kudin, K. N.; Burant, J. C.; Millam, J. M.; Iyengar, S. S.; Tomasi, J.; Barone, V.; Mennucci, B.; Cossi, M.; Scalmani, G.; Rega, N.; Petersson, G. A.; Nakatsuji, H.; Hada, M.; Ehara, M.; Toyota, K.; Fukuda, R.; Hasegawa, J.; Ishida, M.; Nakajima, T.; Honda, Y.; Kitao, O.; Nakai, H.; Klene, M.; Li, X.; Knox, J. E.; Hratchian, H. P.; Cross, J. B.; Bakken, V.; Adamo, C.; Jaramillo, J.; Gomperts, R.; Stratmann, R. E.; Yazyev, O.; Austin, A. J.;

Cammi, R.; Pomelli, C.; Ochterski, J. W.; Ayala, P. Y.; Morokuma, K.; Voth, G. A.; Salvador, P.; Dannenberg, J. J.; Zakrzewski, V. G.; Dapprich, S.; Daniels, A. D.; Strain, M. C.; Farkas, O.; Malick, D. K.; Rabuck, A. D.; Raghavachari, K.; Foresman, J. B.; Ortiz, J. V.; Cui, Q.; Baboul, A. G.; Clifford, S.; Cioslowski, J.; Stefanov, B. B.; Liu, G.; Liashenko, A.; Piskorz, P.; Komaromi, I.; Martin, R. L.; Fox, D. J.; Keith, T.; Al-Laham, M. A.; Peng, C. Y.; Nanayakkara, A.; Challacombe, M.; Gill, P. M. W.; Johnson, B.; Chen, W.; Wong, M. W.; Gonzalez, C.; Pople, J. A. *Gaussian 03*, revision C.02; Gaussian, Inc.: Wallingford, CT, 2004.

(64) Rappé, A. K.; Casewit, C. J.; Colwell, K. S.; Goddard, W. A., III; Skiff, W. M. *J. Am. Chem. Soc*. **1992**, *114*, 10024.

(65) Jordanides, X. J.; Lang, M. J.; Song, X. Y.; Fleming, G. R. *J. Phys. Chem. B* **1999**, *103*, 7995.

(66) Alden, R. G.; Johnson, E.; Nagarajan, V.; Parson, W. W.; Law, C. J.; Cogdell, R. G. *J. Phys. Chem. B* **1997**, *101*, 4667.

(67) Linnanto, J.; Korppi-Tommola, J. E. I.; Helenius, V. M. *J. Phys. Chem. B* **1999**, *103*, 8739.

(68) Hasegawa, J.; Ohkawa, K.; Nakatsuji, H. *J. Phys. Chem. B* **1998**, *102*, 10410.

(69) (a) Becke, A. D. *J. Chem. Phys*. **1993**, *98*, 5648. (b) Lee, C.; Yang, W.; Parr, R. G. *Phys. Rev. B* **1988**, *37*, 785.

(70) Frähmcke, J. S.; Walla, P. J. *Chem. Phys. Lett.* **2006**, *430*, 397.

(71) Georgakopoulou, S.; Frese, R. N.; Johnson, E.; Koolhaas, C.; Cogdell, R. J.; van Grondelle, R.; van der Zwan, G. *Biophys. J.* **2002**, *82*, 2184.

(72) Georgakopoulou, S.; van Grondelle, R.; van der Zwan, G. *J. Phys. Chem. B* **2006**, *110*, 3344.

(73) Novoderezhkin, V. I.; Palacios, M. A.; van Amerongen, H.; van Grondelle, R. *J. Phys. Chem. B* **2005**, *109*, 10493.

(74) Jang, S.; Newton, M. D.; Silbey, R. J. *J. Phys. Chem. B* **2007**, *111*, 6807.

(75) Knox, R. S.; Spring, B. Q. *Photochem. Photobiol*. **2003**, *77*, 497.